agronomy

MDPI

Article

A Dynamic Process-Based Method for Screening Salt-Tolerant and High-Yielding Crop Varieties

Xueer Qin [1,2], Baoying Shan [3,4], Jili Liu [5], Chenglong Zhang [1,2,*], Weishu Wang [1,2], Chaozi Wang [1,2] and Zailin Huo [1,2]

[1] State Key Laboratory of Efficient Utilization of Agricultural Water Resources, China Agricultural University, Beijing 100083, China; qinxueer@cau.edu.cn (X.Q.); wws0208@cau.edu.cn (W.W.); chaoziwang@cau.edu.cn (C.W.); huozl@cau.edu.cn (Z.H.)
[2] Center for Agricultural Water Research in China, China Agricultural University, Beijing 100083, China
[3] Research Unit Knowledge-Based System, Ghent University, 9000 Ghent, Belgium; baoying.shan@ugent.be
[4] Hydro-Climatic Extremes Lab, Ghent University, 9000 Ghent, Belgium
[5] College of Ecology and Environment, Ningxia University, Yinchuan 750021, China; tim11082003@163.com
* Correspondence: zhangcl1992@cau.edu.cn

Abstract: Maize, the most important cereal crop worldwide, is moderately sensitive to salt stress. Given the challenges of soil salinization, developing methods to screen and cultivate salt-tolerant maize varieties is vital for enhancing food security. Among the options, process model-based assisted screening is an effective method for faster and more thorough screening of salt-tolerant varieties. In this study, a method for quickly screening salt-tolerant and high-yielding crop varieties is proposed by combining a coupled model of crop growth and water–salt response with fitness function. Then, this method was applied to the saline areas of the Hetao Plain in China to demonstrate its applicability. This study includes three parts. Firstly, field trial data from 10 commonly grown maize varieties in Hetao Plain (i.e., Xianyu 335, Yinyu 238, Jindan 73, Deke 622, DK-815, Heyu 157, Xianyu 1321, Jinrun 919, Tianci 19, and Xianyu 1225) were used to calibrate the model for different maize varieties. Moreover, model accuracy was evaluated using four indexes including the regression coefficient (b), coefficient of determination (R^2), root mean square error (RMSE), and Nash–Sutcliffe efficiency coefficient (NSE). Secondly, scenario simulations were conducted using the calibrated model by setting nine initial salinity scenarios to simulate daily dynamic crop growth and soil water–salt changes for the 10 maize varieties. Finally, salt-tolerant and high-yielding maize varieties were screened based on the fitness function method during crop growth periods. The results showed that the simulation model was applicable and functioned effectively for all 10 maize varieties in the region, with the determination coefficient (R^2) and Nash–Sutcliffe efficiency coefficient (NSE) of simulated plant height and leaf area index being above 0.90. Furthermore, the R^2 of soil water content, soil electrical conductivity, and groundwater depth are 0.51, 0.52, and 0.60, respectively. Afterward, the fitness function values were calculated to bridge the linkage between simulated indicators and scenarios to screen varieties step by step according to the predetermined percentage of screening. Jindan 73, Xianyu 1225, and DK-815 were eventually determined as the most suitable salt-tolerant and high-yielding maize varieties. Therefore, the above results show that the proposed method is suitable for saline crop variety screening with flexibility and applicability.

Keywords: maize; scenario simulation; fitness function; variety screening; salt tolerant and high yielding; process-based model

check for updates

Citation: Qin, X.; Shan, B.; Liu, J.; Zhang, C.; Wang, W.; Wang, C.; Huo, Z. A Dynamic Process-Based Method for Screening Salt-Tolerant and High-Yielding Crop Varieties. *Agronomy* **2024**, *14*, 1649. https://doi.org/10.3390/agronomy14081649

Academic Editor: Manish K. Pandey

Received: 30 June 2024
Revised: 24 July 2024
Accepted: 25 July 2024
Published: 27 July 2024

Copyright: © 2024 by the authors. Licensee MDPI, Basel, Switzerland. This article is an open access article distributed under the terms and conditions of the Creative Commons Attribution (CC BY) license (https://creativecommons.org/licenses/by/4.0/).

1. Introduction

Soil salinization is a critical challenge in agricultural development, severely impacting crop yields globally [1]. Such an adverse issue mainly results from an imbalance of the soil water movement and salt transport caused by low precipitation and high evapotranspiration. More than three percent of total global soil resources are affected by salt

nowadays [2]. In the meantime, soil salinization will continue to increase due to factors such as global warming and irrational arable land practices. Saline soils are widely distributed on the Earth, covering about 25% of the total land area, and they are found in more than 100 countries [3]. In arid and semi-arid regions, saline soils are especially common, in which evaporation is intense and the amount of rainfall is insufficient for substantial salt leaching. Thus, salinity is one of the main limiting factors for agricultural production in these areas [4]. It poses a continuous threat to food security and crop yields, as well as a significant obstacle to sustainable agriculture. Therefore, adaptive development and utilization of saline soils are essential to maintain agricultural productivity and food security. Currently, saline land improvement measures are mainly categorized into physical, chemical, and biological methods [5]. Physical methods involve washing salts, digging trenches, and drainage. Chemical methods attempt to neutralize the soil's pH value and improve soil properties to prevent salinization. Alternatively, biological methods promote soil desalination and inhibit salinization through the shading effect of plants and the ameliorative action of plant roots [6,7]. Followed by wheat and rice, maize is the world's third most important cereal crop and the largest food producer, which is cultivated in many countries under diverse environmental conditions [8]. Strengthening soil improvement in saline and alkaline lands, exploring the salt-tolerant characteristics of maize, and selecting maize varieties with enhanced salt tolerance are the most direct and effective ways to accelerate the development and utilization of these lands [9]. Therefore, screening and planting high-yielding, salt-tolerant crops is an effective and environmentally sustainable approach to utilizing saline soils.

Most studies on screening salt-tolerant crop varieties rely on field experiments, which are labor-intensive and time-consuming. Additionally, field screening for salt-tolerant and high-yielding varieties is challenging due to the spatial heterogeneity of soil properties and climate variations. Process-based crop models, designed to simulate interactions between phenotypes, environment, and management, are commonly used to evaluate the effects of environmental changes on crop development, growth, and yield [10,11]. In recent decades, crop modeling has become an important tool for evaluating and screening crop varieties [12,13]. The design of ideal genotypes, particularly for various crops and growing conditions, is often known as "model crops" [14–16]. For example, Tao et al. used eight barley simulation models (APSIM, CropSyst, HERMES, MCWLA, MONICA, SIMPLACE, SiriusQuality, and WOFOST) to design and screen ideal genotypes for future climate change. This method was applied in northern Europe and Mediterranean climate zones to identify varieties adapted to future climates. Currently, studies on crop models have reached a practical stage in many countries [17]. For example, the Netherlands' WOFOST (WOrld FOod STudies) and other models are known for being explanatory and mechanistic but less versatile. In contrast, models such as DSSAT and EPIC from the United States are highly applicable, operable, and targeted. Shahhosseini et al. enhanced yield prediction accuracy by integrating the APSIM model with a machine learning model [18]. McNider et al. developed a water deficit index by coupling the hydrological model WaSSI with the crop model DSSAT, reflecting the balance between water demand and supply [19]. Moreover, to tackle the physical processes of water movement and salt transport interlinked with crop growth, coupling crop models with farmland hydrological processes becomes inevitable. For example, Xu et al. proposed a new agroecosystem simulation model to simulate soil water salinity, nitrogen, heat, and crop growth [20]. Wang et al. developed a coupled model of crop growth and water cycle processes in salinized farmland where crop stomatal conductance was involved and quantified by its relationship to meteorological factors, soil water, and salinity. The model is characterized by its computational efficiency and the simplicity of its modules, which make it suitable for use in assisting the screening of salt-tolerant high-yielding varieties [21]. However, few studies have considered water–salt response simulation modeling for crop variety screening on salt-affected soils.

Most of the previous crop variety screening studies were conducted based on indoor or multi-year field trials. Gao et al. evaluated the salt tolerance of 30 maize varieties during

germination using the weighted affiliation function method and cluster analysis. They screened relative germination potential, relative germ length, relative germ weight, and relative germination percentage as evaluation indices in indoor hydroponic experiments [22]. Wang et al. screened the maize plant stage for identification using a field identification method. They evaluated salt tolerance based on plant height, ear fresh weight, stem fresh weight, total fresh weight, and kernel dry weight, employing the weighted subordinate function for a comprehensive evaluation [23]. In contrast, challenges are unavoidable in the experimental screening of salt-tolerant varieties due to time-consuming processes, the inability to evaluate the entire life span, and complex calculations. Furthermore, bridging the linkages among these indicators from experimental screening or simulation models remains a challenge. Therefore, developing a feasible and efficient screening method is crucial for readily supporting agricultural development.

In response to the above concerns, this study aims to develop an effective and rapid screening method for salt-tolerant and high-yielding crop varieties by incorporating a simulation model of crop growth and water–salt response and the concept of fitness function. The fitness function is introduced into the screening process to assess each candidate variety's adaptability and performance objectively. By using the fitness values, the varieties can be quantitatively ranked and the best-performing ones at different growth stages can be identified. To demonstrate its applicability, this method was applied to the saline areas of the Hetao Plain in China.

2. Materials and Methods

2.1. Framework Development

The process model-based framework for screening salt-tolerant and high-yielding crop varieties is obtained by combining the crop growth and water–salt response model with the fitness function. The specific process of the framework is shown in Figure 1. Firstly, using field trial monitoring data, we calibrated the crop growth and water–salt response model parameters for 10 selected salt-tolerant maize varieties and quantitatively assessed various maize metrics using selected evaluation indices. After calibration, multiple scenarios were established to analyze changes in different indicators under varying initial salinity conditions. Lastly, fitness functions for different stages were constructed based on screening process indicators, and the fitness values of various varieties at different growth stages were calculated. These values were then gradually eliminated based on predetermined screening ratios to determine high-yielding and salt-tolerant crop varieties.

2.2. Data Collection

The experimental site (38°50′ N, 106°24′ E) was situated at Qianjin Farm, Pingluo County, Shizuishan City, Ningxia Autonomous Region. The altitude is 1150 m. The average annual precipitation is 205 mm, with annual potential evaporation reaching 1875 mm. Most precipitation occurs between April and October, and the average annual temperature is 9.5 °C, reflecting a typical semi-arid continental climate. The region has abundant sunshine, limited rainfall, and notably diurnal temperature variations. The primary causes of soil salinization in this area are insufficient precipitation and high evaporation [24].

The experiment was conducted in 2023 on maize farmland during the crop growth period (May–September) to monitor crop growth and measure soil water and salinity. It also aimed to monitor the dynamic processes of crop-related indicators, soil salinity, and groundwater depth in farmland ecosystems during this period. Soil water content (SWC) was determined using the drying method by collecting in situ soil samples at corresponding depths every ten days. Plant height, stem thickness, and leaf length and width were measured on three to five representative plants from the field at approximately ten-day intervals. During the growth phase in sunny conditions, the stomatal conductance of the top, middle, and bottom three layers of maize leaves was measured at similar intervals. The soil texture in the experimental field was primarily loamy. To measure the physical characteristics of each soil layer, in situ samples were taken at five depths (20, 40, 60, 80,

and 100 cm) using a ring cutter with a volume of 100 cm^3. A laser particle size analyzer was used to determine soil texture, and Table S1 contains the physical characteristics of the soil.

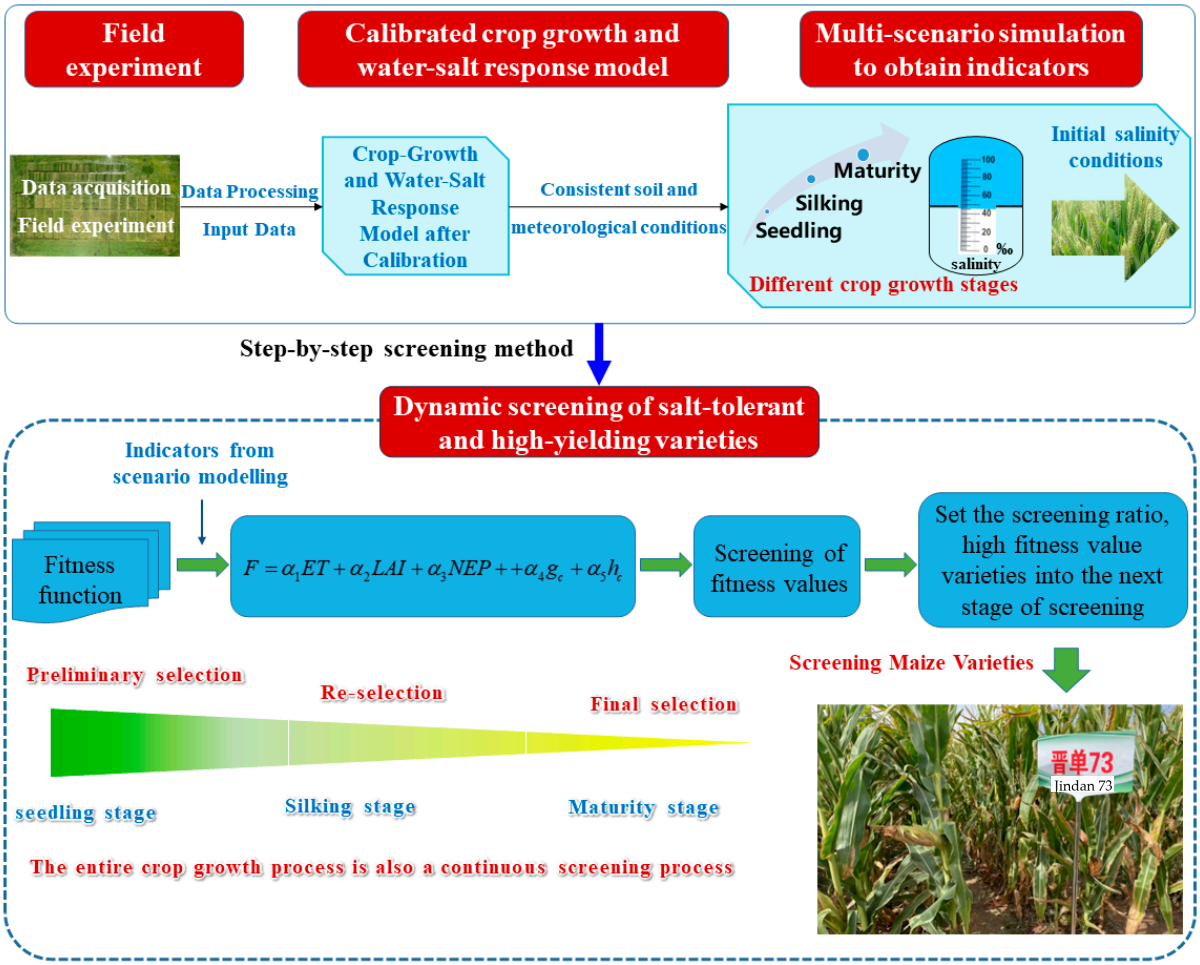


Figure 1. The framework of this study.

The 10 maize varieties tested were sourced from agricultural stores in Yinchuan, Ningxia, all of which are the main local varieties. The 10 commonly grown maize varieties under observation, Xianyu 335, Yinyu 238, Jindan 73, Deke 622, DK-815, Heyu 157, Xianyu 1321, Jinrun 919, Tianci 19, and Xianyu 1225, were sown on 27 April and had a whole growth period of approximately 150 days. Specific crop growth stages are shown in Table S2. The maize was planted with mulching (planting two rows in one row of mulch), with plants spaced 60 cm by 20 cm apart, totaling 80,000 plants per ha. Drip irrigation pipes were placed under the film between the two maize rows. Daily meteorological data, including temperature, radiation, and precipitation, were monitored by the meteorological monitoring station.

Figure S1 shows the meteorological changes at the farm during the 2023 maize growing season. Air temperature (Ta) and photosynthetically active radiation (PAR) both reached their highest levels in May and started to decline in early September. The average PAR during the growing season was 519.75 μmol m^{-2} s^{-1}. The average temperature during the growing season was 22.81 °C, with a maximum of approximately 38 °C and a minimum of approximately 6 °C. The arid climate in the experimental area resulted in a significantly higher saturated water vapor pressure (VPD). Plant transpiration altered the micrometeorological conditions above the farmland, leading to a fluctuating downward trend in VPD above the maize canopy during the reproductive period as the crop canopy expanded, with an average VPD of 1.65 kPa. The carbon dioxide concentration was set at 600 μmol mol^{-1}.

Figure S2 shows the rainfall and irrigation data for the maize farmland during the 2023 crop growth period. The farmland was irrigated 10 times throughout the growing season using drip irrigation, averaging 36 mm per irrigation, a total of 360 mm. The specific irrigation schedule is presented in Table S3. Figure S3 illustrates changes in groundwater depth, which was recharged by irrigation and also contributed to soil moisture and crop water consumption through capillary rise. Groundwater levels increased during the maize growing season, starting at an initial depth of 3.0 m and decreasing to 1.5 m by the end of the growth period.

2.3. Crop Growth and Water–Salt Response Model

The crop growth and water–salt response model used in this study is based on the canopy conductance model, which was improved by the Jarvis model to account for salt stress. It establishes a canopy conductance-based model that couples crop transpiration, photosynthesis, and farmland water cycles while considering the effects of soil water and salt in the crop root zone. This model simulates crop canopy transpiration, photosynthesis, dry matter accumulation, assimilate partitioning, soil water movement, soil salt transport, groundwater depth, and agro-ecosystem water use efficiency [21].

The model enhances the Jarvis model by considering the impact of salinity on stomatal conductance. A model for stomatal conductance (g_s) was developed to account for soil salinity, utilizing the effective leaf area index (LAI_{eff}) to scale up to a canopy conductance (g_c) model. This approach integrates soil water salinity alongside meteorological factors.

$$g_s = f(PAR)\cdot f(VPD)\cdot f(T_a)\cdot f(SWC)\cdot f(EC) \quad (1)$$

$$f(PAR) = PAR/(k_1 + k_1 PAR) \quad (2)$$

$$f(VPD) = 1/(1 + k_3 VPD) \quad (3)$$

$$f(T_a) = k_4 + k_5 T_a + k_6 T_a^2 \quad (4)$$

$$f(SWC) = \left(\theta_v - \theta_{wp}\right) / \left(\theta_{fc} - \theta_{wp}\right) \quad (5)$$

$$f(EC) = 1 - \frac{LAI}{LAI_{\max}} \cdot \frac{EC}{EC_t} \quad (6)$$

$$g_c = g_s \times LAI_{eff} \quad (7)$$

$$LAI_{eff} = LAI/(0.3LAI + 1.2) \quad (8)$$

where θ_v is the volumetric soil water content; θ_{wp} is the wilting soil water content; θ_{fc} is the field water holding capacity; and k_n is an empirical coefficient.

The model simulated evapotranspiration based on the Shuttleworth–Wallace (S–W) method. Solar radiation was allocated to the upper canopy and lower soil using Beer's law. The simulation calculated the canopy latent heat flux (λET), accounting for latent heat fluxes from soil evaporation and plant transpiration. The net productivity of the agroecosystem was calculated using the daytime population and the gross and total respiration (Reco). Crop dry matter accumulation was determined by multiplying the net productivity of the agro-canopy by a CO_2 to glucose conversion factor, while leaf area allocation followed the empirical C4 crop allocation model. The soil water salinity simulation in the model referenced the AquaCrop model's water salinity module, segmented into five layers (0–10 cm, 10–30 cm, 30–50 cm, 50–70 cm, and 70–90 cm). A more detailed explanation of the crop growth and water salt response mode can be seen in Wang et al. [21].

In this study, a total depth of 100 cm was modeled, and it was segmented into five layers (0–20 cm, 20–40 cm, 40–60 cm, 60–80 cm, and 80–100 cm). Initial groundwater depth was set from field observations. The initial value of the SWC of the model was set close to field capacity because irrigation was carried out the day before the initial simulation date. The simulation spanned from early May to mid-September, covering the growth cycle of maize from seedling to maturity.

The crop growth and water–salt response model comprise modules for soil water–salt transport and crop growth. Ten maize varieties (Xianyu 335, Yinyu 238, Jindan 73, Deke 622, DK-815, Heyu 157, Xianyu 1321, Jinrun 919, Tianci 19, and Xianyu 1225) were utilized to calibrate parameters related to crop growth, soil water salinity, and meteorological conditions throughout the entire 2023 life cycle. Key model parameters were determined based on sensitivity analyses reported by [21] highlighting the significant impact of minimum soil surface resistance on evapotranspiration (ET), and the effect of extinction coefficient (*c*) on net ecosystem productivity (NEP) and water use efficiency (WUE). Evaluation of model accuracy was conducted using four indices: regression coefficient (b), coefficient of determination (R^2), root mean square error (RMSE), and Nash–Sutcliffe efficiency coefficient (NSE). Specific model parameters are detailed in Table S4.

R^2 indicates how closely simulated values match measured values, with values ranging from 0 to 1. Higher values of b and R^2 signify better model performance, indicating a strong fit between simulated and measured data. RMSE quantifies model accuracy, with lower values indicating higher accuracy. NSE evaluates the model's reliability, where values closer to 1 denote high model quality and reliability, whereas values near 0 suggest larger simulation errors relative to observations. If NSE is significantly below 0, the model's credibility is compromised. The equations for calculating R^2, RMSE, and NSE are presented as follows:

$$R^2 = \frac{\sum_{i=1}^{n} (O_i - \overline{O})(P_i - \overline{P})}{\sqrt{\sum_{i=1}^{n} (O_i - \overline{O})^2} \sqrt{\sum_{i=1}^{n} (P_i - \overline{P})^2}} \quad (9)$$

$$RMSE = \sqrt{\sum_{i=1}^{n} \frac{(P_i - O_i)^2}{n}} \quad (10)$$

$$NSE = 1 - \frac{\sum_{i=1}^{n} (P_i - O_i)^2}{\sum_{i=1}^{n} (O_i - \overline{O})^2} \quad (11)$$

where: n is the number of observations, P_i and O_i are the simulated and measured values for day i, and $\overline{P}$ and $\overline{O}$ are the average of the simulated and measured values.

2.4. Simulation Scenario Setting

Scenario simulation analysis plays a pivotal role in the screening of salt-tolerant and high-yielding crop varieties. It allows for assessing crop growth across different soil salinity levels, climatic conditions, and other variables. By simulating various scenarios, essential metrics related to crop performance can be derived, thereby facilitating the screening of the most suitable varieties for saline environments. Additionally, scenario simulation entails conducting extensive virtual experiments before actual field trials, which saves time, reduces costs, and enhances selection efficiency. In this study, assuming consistent soil texture and model parameters for water and salt dynamics during simulation, nine salinity scenarios ranging from 2.0 to 6.0 g/kg were established, with a step increment of 0.5 g/kg (i.e., 2.0 g/kg, 2.5 g/kg, 3.0 g/kg, 3.5 g/kg, 4.0 g/kg, 4.5 g/kg, 5.0 g/kg, 5.5 g/kg, and 6.0 g/kg). Detailed salt concentration settings are outlined in Table 1.

Table 1. The nine initial salt level settings in the simulation analysis.

Different Salt Scenarios	Initial Salt Content (g/kg)
D0	2.0
D1	2.5
D2	3.0
D3	3.5
D4	4.0
D5	4.5
D6	5.0
D7	5.5
D8	6.0

2.5. Design of the Fitness Function

The fitness function, which originated from genetic algorithms, is commonly used to estimate the function of the generated population. Theoretically, the highest fitness leads to the greatest chance of contributing to future generations, and the lowest values of fitness are eliminated on the basis of the natural selection process of survival of the fittest. Thus, it is critical to design a logical, consistent, computationally efficient, and versatile fitness function. A typical type of fitness function is the linear function, given by $f(x) = ax + b$, where a and b are constants. The linear fitness function is commonly applied to optimize objective minimization or maximization problems. Other types include exponential, nonlinear, and constrained fitness functions. In practical applications, the design of the fitness function should be based on the specific problems.

Evaluating the salt tolerance of crop varieties based on a single indicator does not accurately reflect the ability of crops to grow under salt stress. When selecting the type of fitness function, it is crucial to consider computational efficiency and the requirement for efficient screening. Therefore, a linear format is chosen for constructing the fitness function, which can be expressed as follows:

$$F = \alpha_1 \mathrm{ET} + \alpha_2 \mathrm{LAI} + \alpha_3 \mathrm{NEP} + + \alpha_4 g_c + \alpha_5 h_c \quad (12)$$

F denotes high-yield salt tolerance, where higher values reflect greater salt tolerance, as all five selected indicators positively correlate with yield. NEP reflects the overall productivity and carbon balance of farmland ecosystems, measured in $gCO_2\ m^{-2}\ d^{-1}$. It directly quantifies the capacity of farmland ecosystems to act as either a source or sink of carbon. A NEP value greater than 0 means the ecosystem absorbs more CO_2 than it releases, making it a carbon sink. Conversely, a negative NEP indicates a carbon source. Canopy conductance (g_c) describes stomatal behavior at the canopy level, influencing crop transpiration and photosynthesis and regulating water vapor and CO_2 exchange between the canopy and the atmosphere. Evapotranspiration (ET) is the water loss from agricultural fields (mm). Leaf area index (LAI) is the total area of plant leaves per unit of land area as a multiple of land area. It is obtained by measuring the leaf length and maximum leaf width of the plant. LAI is measured in $m^2\ m^{-2}$, and h_c is the height of maize plants (m). α_1, α_2, α_3, α_4, and α_5 are the weighting coefficients used in the analysis. Based on the defined fitness function, the fitness function values for each variety at different growth stages were calculated. The simulated index values of LAI, h_c, and g_c were obtained as mean values during the screening stage, and ET and NEP were obtained as cumulative values during the screening stage. Higher fitness degree values indicate better performance at that crop growth stage. Therefore, by using the fitness function calculations, the varieties can be quantitatively ranked and the best-performing ones at different growth stages can be identified. These superior varieties can then be used for the selection and promotion of salt-tolerant and high-yielding crops.

2.6. Weighting Calculations

This study utilizes the coefficient of variation method as part of the objective assignment method to determine the weights. The coefficient of variation method calculates weights based on the information contained in the indicators, highlighting the degree of variation among them. Indicators with greater variations are assigned more significant weights. This method prioritizes the degree of difference among indicators but can be challenging when dealing with many evaluation indicators and objects. Normalizing the indicators before assigning weights is a reliable approach. Therefore, in this study, the original indicator data are first made dimensionless before using the coefficient of variation method. The calculation steps are listed as follows:

(1) Assuming that there are m evaluation objects and n evaluation indicators, construct the raw data matrix X:

$$X = \begin{pmatrix} x_{11} & \cdots & x_{1n} \\ \vdots & \ddots & \vdots \\ x_{m1} & \cdots & x_{mn} \end{pmatrix} \tag{13}$$

(2) The data were normalized using polarization to construct a decision matrix $V = (x_{ij})_{m \times n}$.

If x is an extremely large property:

$$x^* = \frac{x - x_{\min}}{x_{\max} - x_{\min}} \tag{14}$$

If x is an extremely small property:

$$x^* = \frac{x_{\max} - x}{x_{\max} - x_{\min}} \tag{15}$$

(3) Calculation of the coefficient of variation V_j

$$V_j = \frac{\sigma_j}{\overline{x}_j^*} \tag{16}$$

$$\sigma_j = \sqrt{\frac{\sum_{i=1}^{m} (x_{ij}^* - \overline{x}_j^*)^2}{m-1}} \tag{17}$$

$$\overline{x}_j^* = \sum_{i=1}^{m} x_{ij}^* / n \tag{18}$$

where σ_j is the standard deviation of the first evaluation indicator and $\overline{x}_j$ is the mean of the first indicator.

(4) Normalized weight of the j indicator

$$\overline{e}_j = \frac{V_j}{\sum_{j=1}^{n} V_j} \tag{19}$$

3. Results

3.1. Stomatal Response to Salinity

Stomata, as shared pathways for photosynthesis and transpiration, regulate the exchange of carbon dioxide and water vapor between leaves and the atmosphere, thereby affecting the rates of photosynthesis and transpiration in plants. The correlation between maize leaf stomatal conductance (g_s) and soil water salinity is depicted in Figure 2. The study results indicated a robust negative relationship between maize leaf stomatal con-

ductance (g_s) and soil salinity content under nearly uniform meteorological conditions. As the $EC_{1:5}$ value increased, maize leaf g_s exhibited a declining trend. Further analysis revealed that maize stomata were significantly impacted by salinity during the seedling stage, with reduced impact during the jointing and silking stages. Stomatal sensitivity to salinity increases again during the maturity stage. Rooted in a sunflower crop model based on canopy conductance, this study also confirms the model's suitability for maize, showing a comparable negative correlation response to salinity as seen in sunflowers [21].

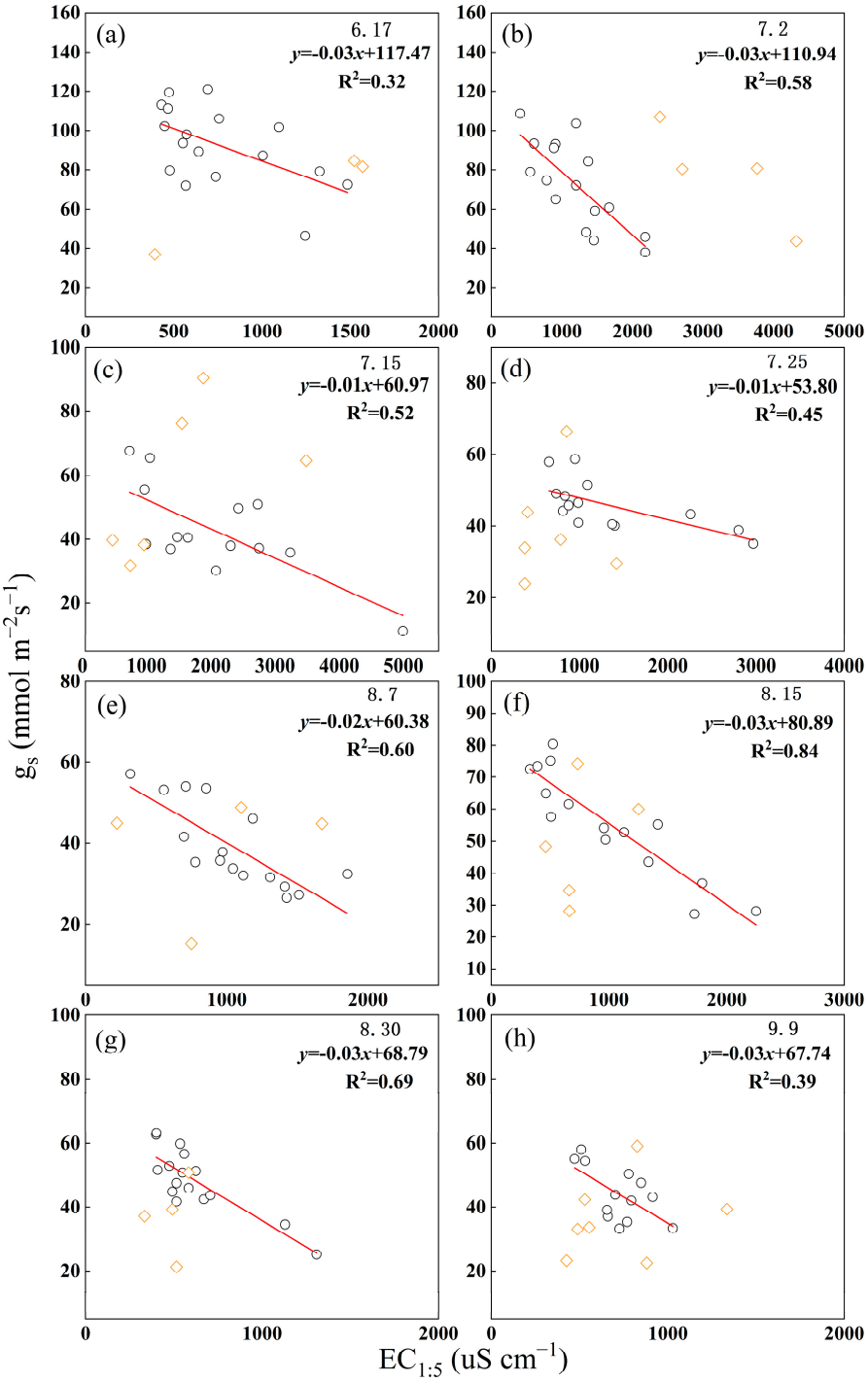


Figure 2. Response relationship between g_s and soil salinity in the root zone of maize. Note: $EC_{1:5}$ is the electrical conductivity of a solution with a soil/water ratio of 1:5, measured by an electrical conductivity meter (FE38-Meter. Mettler-Toledo Instruments (Shanghai) Co., Ltd., Shanghai, China).

3.2. Model Calibration

The calibration of parameters for each maize variety was conducted individually through experimental data. Table S4 outlines the essential varietal parameters and their associated soil parameter values for the 10 maize varieties.

The results indicate that the model effectively simulated the LAI. Figure S4 shows the simulated dynamics of maize LAI throughout 2023 using the calibrated model. The R^2 values were all above 0.91, the mean RMSE was 0.53 m^3 m^{-3}, and the NSE values were all above 0.90. Figure S5 shows the results of dynamic changes in plant height in 2023 simulated by the simulation model. The model effectively simulated the changes in plant height throughout the entire growth period. Figure S6 presents the model's simulation results of dynamic soil water content (SWC) at various depths in maize farmland during 2023. The results indicate that the model accurately captures the daily-scale dynamics of SWC, with R^2 values exceeding 0.51, RMSE values less than 0.03 cm^3 cm^{-3}, and an average NSE of 0.54. The model simulation results depicted in Figure S7 illustrate the dynamic changes in soil electrical conductivity (EC) values within the root zone of maize farmland crops during 2023. The results indicate that the model effectively captures the daily-scale variations in EC across different root zone depths, achieving R^2 values consistently above 0.83. The model's performance is reflected in a mean RMSE of 0.67 ds m^{-1} and a mean NSE of 0.39. The model's low accuracy in simulating soil water salinity is mainly because the measured values are from various soil samples for calibration, rather than continuously monitored sensor data. Additionally, the experimental site showed non-uniform salinity distribution. Nonetheless, the model's simulations generally reflect the patterns of water and salt changes in farmland. For varietal screening studies, identical soil parameters were assumed for all 10 maize varieties, with the assumption of uniform soil salinity during the simulations. Figure S8 shows the comparison between the model's simulation of the dynamic changes in groundwater depth in maize farmland during 2023 and sensor measurements. The results indicate that the model reliably simulates the daily variations in groundwater depth. The evaluation metrics for model calibration are provided in Table S5.

3.3. Simulation Results of Salt Scenarios

For each scenario, the simulations showed that LAI decreased as salinity increased, but plant height was not affected by salinity changes. Figure 3 presents the mean LAI and plant height (h_c) changes during the growth stages of 10 maize varieties, based on the crop growth and water–salt response model under different salinity scenarios. Among the 10 maize varieties, the LAI of Jindan 73 was the largest and that of Deke 622 was the smallest at the seedling–jointing stage. The LAI of Xianyu 1225 was the largest and that of Deke 622 was the smallest at the jointing–silking stage. The LAI of Jindan 73 was the largest and that of Xianyu 335 was the smallest at the silking–maturity stage. The plant height of DK-815 was the largest and that of Yinyu 238 was the smallest at the seedling–jointing stage, the plant height of DK-815 was the largest and that of Yinyu 238 was the smallest, and the plant height of Xianyu 1225 was the largest and that of Deke 622 was the smallest at the silking–maturity stage. When the salinity increased from 2.0‰ to 6.0‰, the LAI of 10 maize varieties in the seedling–jointing stage decreased less, and that of Yinyu 238 varieties in the jointing–silking stage decreased the most, by 0.47 m^2 m^{-2}. DK-815 varieties decreased the least, by 0.20 m^2 m^{-2}. Yinyu 238 varieties in the silking–maturity stage decreased the most, by 0.89 m^2 m^{-2}. The DK-815 variety had the smallest decrease of 0.30 m^2 m^{-2}.

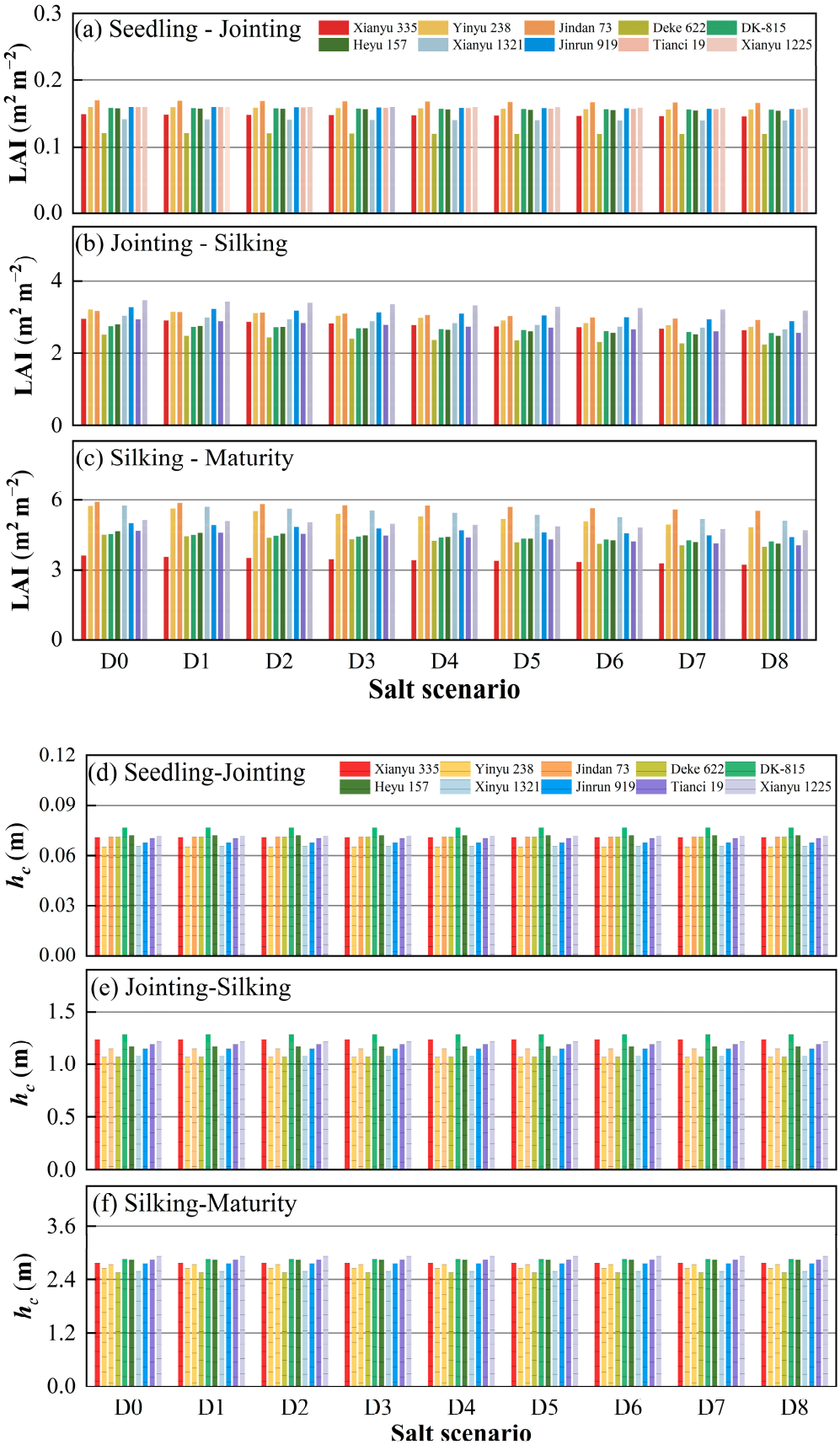


Figure 3. Changes in mean LAI and h_c under different salinity scenarios and growth stages.

Figure 4 shows the changes in the average ET of 10 maize varieties, simulated by the crop growth and water–salt response model under various salinity scenarios and growth stages. The results demonstrated that average ET declined as salinity increased. Among the 10 maize varieties, Jinrun 919 had the highest ET and Xianyu 335 had the lowest ET during the seedling–jointing stage. The ET of Jinrun 919 was the largest and that of Heyu 157 was the smallest at the stage of jointing–silking; the ET of Jindan 73 was the largest and that of Xianyu 335 was the smallest at the stage of silking–maturity. When salinity increased from 2.0‰ to 6.0‰, Heyu 157 showed the greatest decrease of 2.67 mm at the seedling–jointing stage, and Xianyu 1225 showed the smallest decrease of 1.79 mm. Yinyu 238 had the largest drop of 30.35 mm from the jointing–silking stage, and DK-815 had the smallest drop of 13.52 mm. Yinyu 238 had the largest drop of 14.76 mm from the silking–maturity stage, and Jindan 73 had the smallest drop of 4.54 mm.

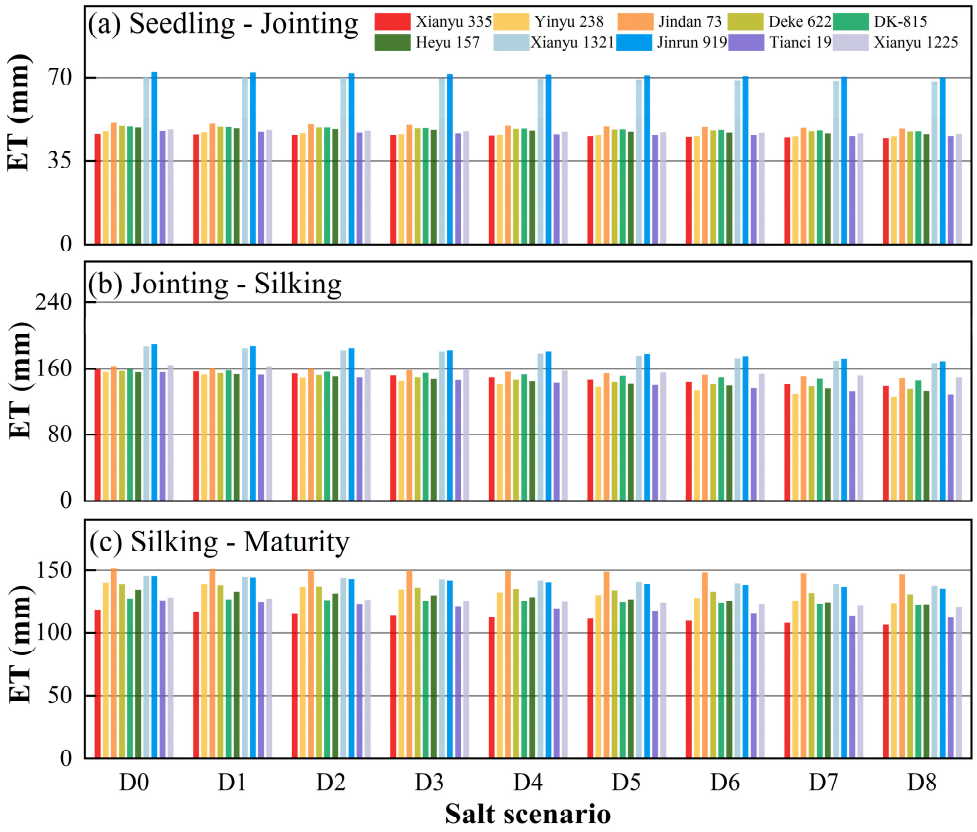


Figure 4. Changes in mean crop ET under different salinity scenarios and growth stages.

Figure 5 shows the variation in cumulative NEP over the growth period of 10 maize varieties under different salinity scenarios and different growth stages. The simulation results showed that the cumulative NEP decreased with increasing salinity, and among the 10 maize varieties, the NEP of Jindan 73 was the largest and that of Xianyu 335 was the smallest at the seedling–jointing stage. The NEP of Xianyu 1225 was the largest and that of Yinyu 238 was the smallest at the jointing–silking stage. The NEP of Jindan 73 was the largest and that of Xianyu 335 was the smallest at the silking–maturity stage. When salinity was increased from 2.0‰ to 6.0‰, at the seedling–jointing stage, Heyu 157 showed the greatest decrease, with a decrease of 10.91 $gCO_2\ m^{-2}d^{-1}$, and Xianyu 1321 showed the smallest decrease, with a decrease of 8.42 $gCO_2\ m^{-2}d^{-1}$. Yinyu 238 had the largest decrease at the jointing–silking stage, with a decrease of 204.10 $gCO_2\ m^{-2}d^{-1}$, and DK-815 had the smallest decrease, with a decrease of 97.34 $gCO_2\ m^{-2}d^{-1}$. Yinyu 238 had the largest decrease at the silking–maturity stage, with a decrease of 190.82 $gCO_2\ m^{-2}d^{-1}$, and Jindan 73 had the smallest decrease, with a decrease of 51.96 $gCO_2\ m^{-2}d^{-1}$.

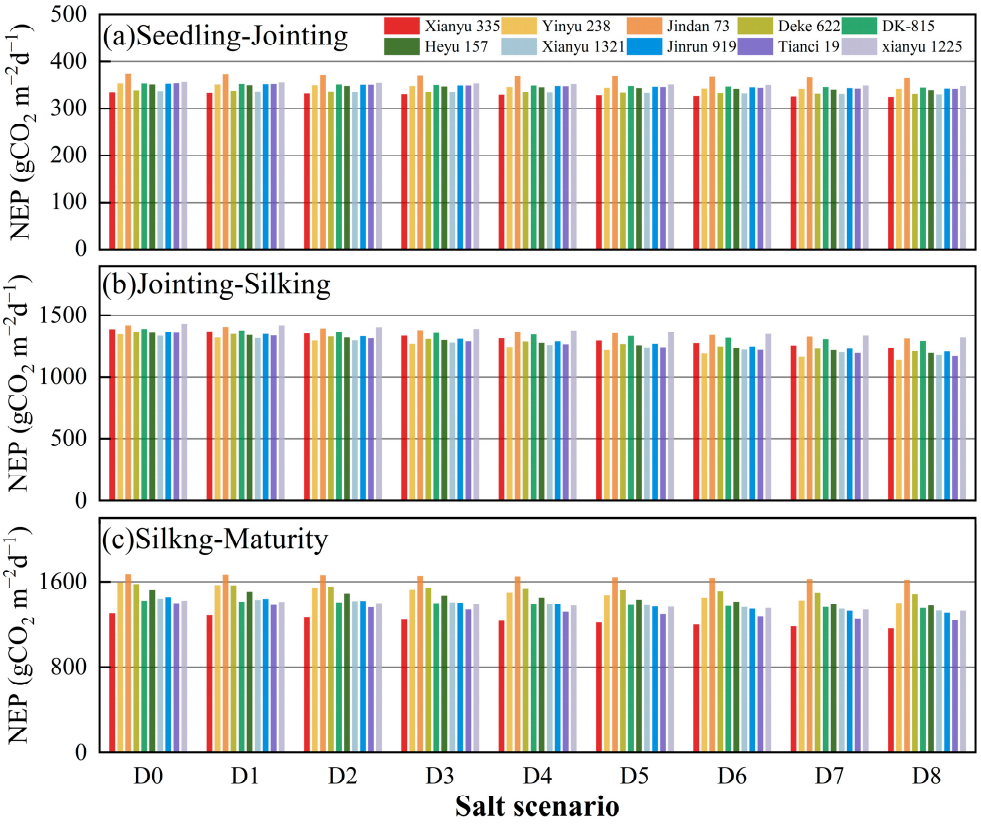


Figure 5. Changes in mean NEP under different salinity scenarios and growth stages.

Figure 6 shows the changes in mean canopy conductance g_c over the growth period of 10 maize varieties simulated by the model under different salinity scenarios and at different growth stages. The simulation results showed that canopy conductance g_c decreased with increasing salinity, and among the 10 maize varieties, g_c was greatest in Jindan 73, DK-815, and Xianyu 1225, and smallest in Deke 622, Yinyu 238, and Xianyu 1321 at the seedling–jointing stage. The g_c of Jindan 73 and Xianyu 1225 was the largest and that of Yinyu 238 and Tianci 19 was the smallest at the jointing–silking stage. The NEP of Jindan 73 and Xianyu 1225 was the largest and that of Xianyu 335 was the smallest at the silking–maturity stage. When the salinity increased from 2.0‰ to 6.0‰, the changes were small in the seedling–jointing stage and the Yinyu 238 variety had the largest decrease in the jointing–silking stage, with a decrease of 0.55 mm s^{-1}, while the DK-815 variety had the smallest decrease, with a decrease of 0.26 mm s^{-1}. The Yinyu 238 variety had the largest decrease in the silking–maturity stage, with a decrease of 0.64 mm s^{-1}, and the Jindan 73 variety had the smallest decrease, with a decrease of 0.21 mm s^{-1}. The largest decrease was 0.64 mm s^{-1} for Yinyu 238, and the smallest decrease was 0.21 mm s^{-1} for Jindan 73.

The coefficient of variation method was used to assign weights to each indicator, which were then integrated into the fitness function to produce the fitness function for each growth stage. First, this study was conducted to compare the performance of different varieties in terms of salt tolerance and high yield at different stages using fitness function values. In this study, the fitness function values for each variety at different growth stages are obtained by the mean value of nine simulated scenarios. The range of salt scenarios set was 2.0–6.0 g/kg, including nine salt gradient scenarios, 2.0 g/kg, 2.5 g/kg, 3.0 g/kg, 3.5 g/kg, 4.0 kg/kg, 4.5 g/kg, 5.0 g/kg, 5.5 g/kg, and 6.0 g/kg, which reflected the actual local conditions of slight to moderate salinity. To comprehensively express the fitness functions corresponding to the simulation results of the nine scenarios, the mean values are used to express the comprehensive salt tolerance property of each variety under salt stress. Moreover, the simulated index values of LAI, h_c, and g_c were obtained as mean

values during each screening stage, and ET and NEP were obtained as cumulative values during the screening stage.

Seedling–jointing stage:

$$F = 0.35\text{ET} + 0.11\text{LAI} + 0.15\text{NEP} + 0.17g_c + 0.22h_c \quad (20)$$

Jointing–silking stage:

$$F = 0.24\text{ET} + 0.07\text{LAI} + 0.20\text{NEP} + 0.21g_c + 0.29h_c \quad (21)$$

Silking–maturity stage:

$$F = 0.20\text{ET} + 0.20\text{LAI} + 0.23\text{NEP} + 0.13g_c + 0.25h_c \quad (22)$$

For example, Table S6 and Figure 7 display the standardized values alongside the fitness values for the seedling–jointing stage.

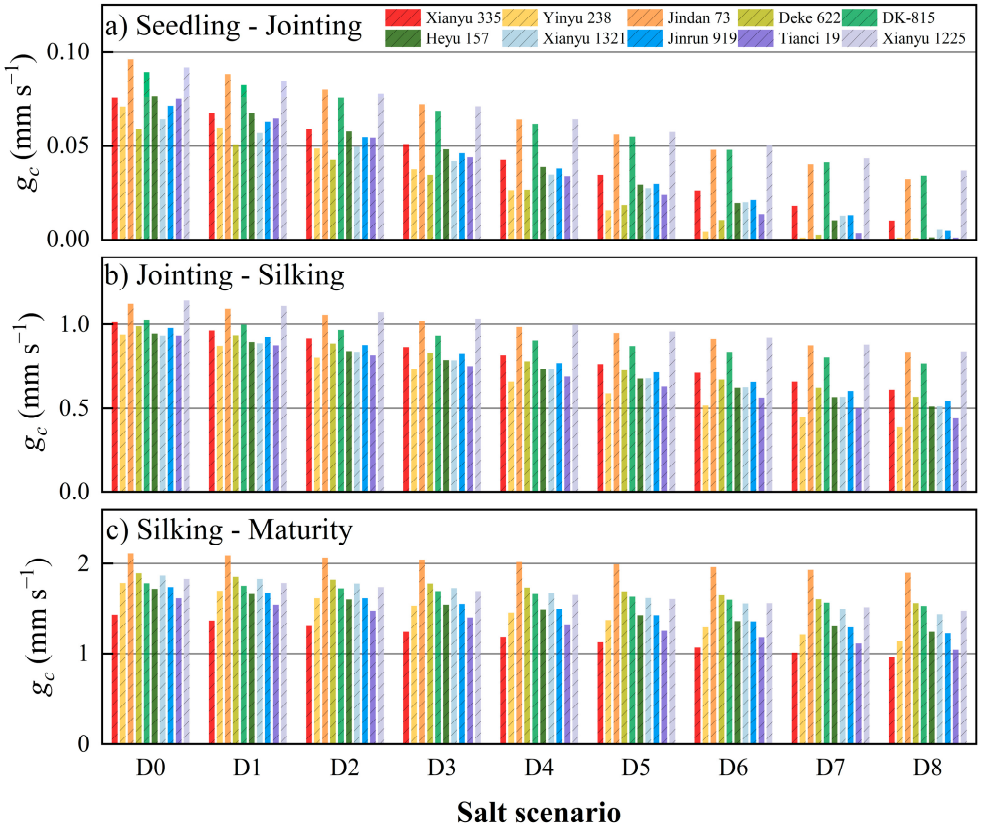


Figure 6. Changes in g_c in agricultural fields under different salinity scenarios and growth stages. Calculation of the Fitness Function.

3.4. Screening Results of Salt-Tolerant and High-Yielding Varieties

The 90 simulated salinity scenarios were comprehensively evaluated using the fitness function method. Different growth stages were employed for phase-by-phase screening. The average fitness function value from each salinity scenario was used as the total fitness value for each variety, serving as the basis for the screening sequence. The total fitness values for each variety are shown in Figure 8.

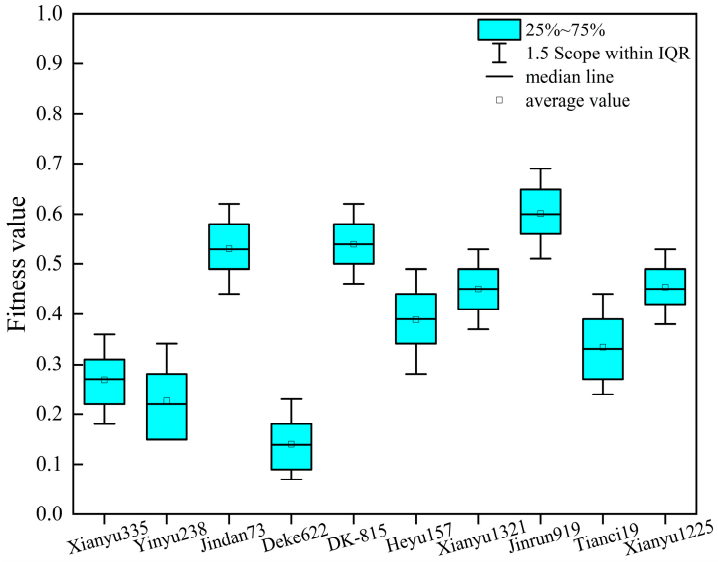
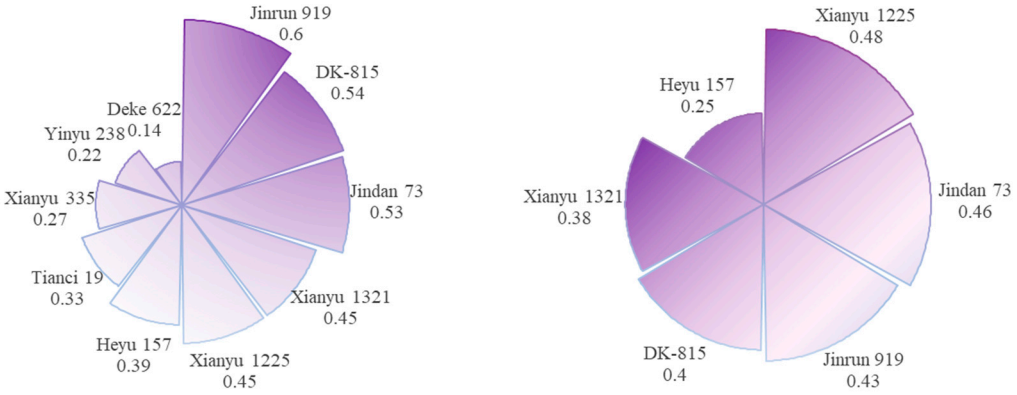
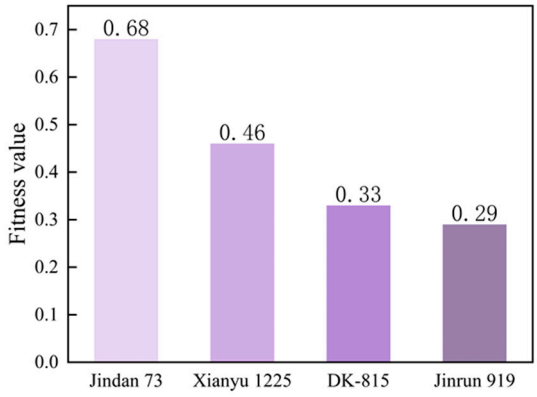


Figure 7. Fitness function values of each maize variety for each salinity scenario at the seedling–jointing stage.



Seedling–jointing fitness values

Jointing–silking fitness values



Silking–maturity fitness values

Figure 8. Fitness values at each growth stage.

Firstly, a 40% phase-out rate was set at the seedling–jointing stage, and the fitness values of Jinrun 919, DK-815, Jindan 73, Xianyu 1321, Xianyu 1225, Heyu 157, Tianci 19, Xianyu 335, Yinyu 238, and Deke 622 were 0.60, 0.54, 0.53, 0.45, 0.45, 0.39, 0.33, 0.27, 0.22, and 0.14, respectively, thus eliminating the last four (i.e., Tianci 19, Xianyu 335, Yinyu 238, and Deke 622) with the lowest fitness values, leaving the top six varieties (i.e., Jindan 73,

DK815, Heyu 157, Xianyu 1321, Jinrun 919, and Xianyu 1225) in the next stage of screening. Secondly, the elimination rate of 1/3 was set at the stage of jointing–silking. The fitness values of Xianyu 1225, Jindan 73, Jinrun 919, DK815, Xianyu 1321, and Heyu 157 were 0.48, 0.46, 0.43, 0.40, 0.38, and 0.25, respectively, resulting in the elimination of the Xianyu 1321 and Heyu 157 varieties, with the remaining varieties entered into the next stage of screening. Finally, the four remaining maize varieties at the silking–maturity stage, Jindan 73, Xianyu 1225, DK-815, and Jinrun 919, had fitness values of 0.68, 0.46, 0.33, and 0.29, which set up an elimination rate of 1/4, eliminating Jinrun 919, and ultimately screening Jindan 73, Xianyu 1225, and DK815 as salt-tolerant, high-yielding varieties.

4. Discussion

4.1. Model Selection and Applicability

Screening salt-tolerant varieties through field experiments is often expensive, time-consuming, and subject to temporal and spatial variations that can affect the results. Therefore, modeling is necessary to infer outcomes across different times and locations. Crop modeling, which integrates physiological, ecological, and mathematical applications, significantly aids decision-making in crop variety promotion. Nowadays, studies on crop models have reached a practical stage globally. The WOFOST model from the Netherlands is more explanatory and mechanistic but less versatile. Meanwhile, the DSSAT and EPIC models from the United States are noted for their high practicality, operability, and relevance [25–30]. Meanwhile, the integration of crop models with hydrological models is increasingly vital for effective agricultural water management. This study utilizes a canopy conductance-based crop growth and water–salt response model that accurately simulates crop growth and soil water–salt dynamics on saline and alkaline soils. Known for its regional adaptability, swift operation, and straightforward structure, the model aligns perfectly with the goal of swiftly screening salt-tolerant varieties. Evaluation metrics affirm the model's ability to accurately simulate maize growth, soil water dynamics, and salt changes, essential for identifying salt-tolerant and high-yielding varieties.

4.2. Advantages and Effectiveness of Screening Salt-Tolerant Varieties

Existing studies indicate that maize is a moderately sensitive crop and its resistance to salt is weak [9]. The salt tolerance of maize is a multifaceted trait that cannot be accurately evaluated using a single indicator alone. Moreover, evaluating crop varieties' salt tolerance based on a single indicator may not provide a complete picture of their ability to withstand salt stress. Recent advancements have introduced comprehensive evaluations using multivariate statistical methods. These include the salt tolerance association function, salt tolerance cluster analysis, and grey correlation analysis. These methods enable a thorough assessment of crop performance under diverse salt conditions. However, determining the salt tolerance of crops for screening purposes can be challenging without extensive experimental data and complex statistical methods such as affiliation function or cluster analysis. The process of screening salt-tolerant and high-yielding varieties in trials is often time-consuming and labor-intensive, typically focusing on the germination and seedling stages, potentially overlooking later-stage salt tolerance in some varieties. Each maize variety exhibited distinct responses to varying salt stress levels, with Jindan 35, Xianyu 1225, and DK-815 demonstrating relatively robust growth performance. In this study, five indicators, ET, NEP, LAI, h_c, and g_c, derived from a process-based model, were utilized, and a comprehensive analysis was conducted to identify salt-tolerant and high-yielding maize varieties across different growth stages. Utilizing model-assisted screening ensures a thorough assessment of indicator changes throughout different growth stages, mitigating the risk of prematurely excluding potentially salt-tolerant varieties.

Following scenario modeling, numerous indicators of crop growth and water and salt transport were obtained, and it is urgently needed to establish linkages between these indicators to distinguish differences between scenarios and varieties. To simplify and ensure reliable evaluation of salt-tolerant and high-yielding varieties, this study proposes

a mathematical formula based on the fitness function. By using the fitness function, the varieties can be quantitatively ranked and the best-performing ones at different growth stages can be identified. The coefficient of variation method was utilized to assign weights to these indicators. The fitness value reflects both salt tolerance and high yield attributes, with higher values indicating greater attributes. To facilitate quick screening, salt-tolerant and high-yielding maize varieties are gradually screened based on growth stages. In this study, 10 maize varieties were screened for salt tolerance and high yield using a process-based model through a fitness function, and Jindan 73, Xianyu 1225, and DK-815 were identified as the most salt-tolerant and high-yielding varieties by computing their fitness values. These identified varieties have a proven record of high yield in local saline soils. In summary, the screening method and results of salt-tolerant and high-yielding varieties designed in this study lay the foundation for reducing the difficulty and improving the accuracy of salt-tolerance evaluation.

5. Conclusions

This study proposed a new method for screening salt-tolerant and high-yielding crop varieties using a process-based model and fitness function, which was then applied to field maize in the arid and saline regions of the Hetao Plains. Moreover, an efficient fitness function screening method was designed that links indicators via process-based model simulations, proving more effective than previous studies. The results revealed that:

(1) The R^2 of the LAI of the 10 maize varieties (Jinrun 919, DK815, Jindan 73, Xianyu 1321, Xianyu 1225, Heyu 157, Tianci 19, Xianyu 335, Yinyu 238, and Deke 622) was greater than 0.91, the mean value of RMSE was 0.53 m^3 m^{-3}, and the NSE was greater than 0.90 for all varieties. The R^2 of plant height was greater than 0.95, the mean value of RMSE was 0.25 m, and the NSE also exceeded 0.92. The R^2 of soil water content was greater than 0.51, the mean value of RMSE was less than 0.03 cm^3 cm^{-3}, and the mean value of NSE was 0.54. The R^2 of soil conductivity was greater than 0.83, the mean value of RMSE was 0.67 ds m^{-1}, and the mean value of NSE was 0.39. The R^2 of groundwater burial depth was 0.60, the RMSE was 0.23 m, and the NSE reached 0.59. The model was able to effectively simulate the changes in the LAI, plant height, and daily soil water and salinity of maize.

(2) Screening of salt-tolerant and high-yielding maize varieties based on the fitness values.

Using the crop growth and water–salt response model, indicator data (ET, LAI, NEP, g_c, and h_c) were obtained by simulating different salinity scenarios. A linear fitness function was proposed to integrate these indicators, allowing for the quantitative screening of salt-tolerant and high-yielding maize varieties. The screening results indicated that:

(1) At the seedling to jointing stage, the fitness values of the 10 maize varieties were 0.60, 0.54, 0.53, 0.45, 0.45, 0.39, 0.33, 0.27, 0.22, and 0.14, and the elimination rate was set at 2/5 to phase out the remaining varieties for the next stage. The Xianyu 335, Deke 622, Yinyu 238, and Tianci 19 varieties were eliminated, and the remaining varieties went to the next stage of screening.

(2) At the stage of jointing–silking, the fitness values of the remaining six maize varieties (Xianyu 1225, Jindan 73, Jinrun 919, DK815, Xianyu 1321, and Heyu 157) were 0.48, 0.46, 0.43, 0.40, 0.38, and 0.25, and a 1/3 elimination rate was set to phase out the varieties of Xianyu 1321 and Heyu 157, with the remaining varieties going to the next stage of screening

(3) At the silking–maturity stage, the fitness values of the remaining four maize varieties (Jindan 73, Xianyu 1225, DK-815, and Jinrun 919) were 0.68, 0.46, 0.33, and 0.29, which set up an elimination rate of 1/4, eliminating the Jinrun 919 variety, and finally establishing Jindan 73, Xianyu 1225, and DK-815 as salt-tolerant and high-yielding varieties.

Supplementary Materials: The following supporting information can be downloaded at: https://www.mdpi.com/article/10.3390/agronomy14081649/s1, Figure S1: Variations of daily average net photosynthetically active radiation (PAR), air temperature (Ta), radiation (Rn), water vapor pressure deficit (VPD), frictional wind speed (u*) and horizontal wind speed (u) of maize; Figure S2: Variations of irrigationnt (I) and rainfall (P) during maize growth period; Figure S3: Variations of groundwater depth during maize growth period; Figure S4: Comparison of simulated and measured leaf area index of maize; Figure S5: Comparison of simu-lated and measured plant height of maize; Figure S6: Comparison between simulated results and measured values of soil water content in different depth layers during maize growth period; Figure S7: Comparison of simulated results and measured values of soil electrical conductivity in root zone during maize growth period; Figure S8: Simulation results of groundwater depth in maize growth period and comparison with measured values; Table S1: Soil physical properties in maize fields; Table S2: Experiment on the growth period of maize varieties; Table S3: Maize irrigation schedule in 2023; Table S4: Specifies the main parameters of the model; Table S5: Values of fitness indicators related to model calibration; Table S6: Standardized values and fitness values.

Author Contributions: Conceptualization, X.Q. and B.S.; Methodology, X.Q. and C.Z.; Software, W.W.; Validation, X.Q. and J.L.; Formal analysis, X.Q.; Investigation, J.L.; Data curation, C.Z. and W.W.; Writing—original draft, X.Q., B.S. and C.Z.; Writing—review & editing, B.S.; Visualization, C.W.; Supervision, C.Z.; Funding acquisition, Z.H. All authors have read and agreed to the published version of the manuscript.

Funding: This study has been supported by the National Key R & D Program of China (No. 2021YFD1900603) and the National Natural Science Foundation of China (No. 52279050).

Data Availability Statement: The original contributions presented in the study are included in the article/Supplementary Material, further inquiries can be directed to the corresponding author.

Conflicts of Interest: The authors declare no conflict of interest.

References

1. Hillel, D. *Out of the Earth: Civilization and the Life of the Soil*; University of California Press: Oakland, CA, USA, 1992.
2. FAO. *Management of Salt Affected Soils: Soil Management under FAO Soils Portal*; FAO: Rome, Italy, 2002.
3. Sun, H.; Lu, H.; Chu, L.; Shao, H.B.; Shi, W.M. Biochar applied with appropriate rates can reduce N leaching, keep N retention, and not increase NH_3 volatilization in a coastal saline soil. *Sci. Total Environ.* **2017**, *575*, 820–825. [CrossRef] [PubMed]
4. Dai, X.; Huo, Z.; Wang, H. Simulation for the response of crop yield to soil moisture and salinity with artificial neural network. *Field Crops Res.* **2011**, *121*, 441–449. [CrossRef]
5. Zhao, X.; Han, N.; Wang, H.; Zhang, Y. Research Progress of Saline Soil Improvement Technology. *Chin. Agric. Sci. Bull.* **2016**, *32*, 113–116.
6. Wang, L.; Pan, J.; Zhao, J.; Li, M.; Zhang, H.; Wang, C.; Dong, Y.; Xiao, H. Improving effect of different amendments on coastal saline-alkali soil. *Hubei Agric. Sci.* **2024**, *63*, 31–35.
7. Zhao, W.; Wang, S.; Liu, L.; Xiao, J.; Wang, S.; Tang, L.; Chen, G. Effect of biochar Amendment on saline-alkaline Soil Amelioration and Plant Growth: A Literature Review. *Chin. J. Soil Sci.* **2024**, *55*, 551–561.
8. Akram, M.; Ashraf, M.Y.; Ahmad, R.; Waraich, E.A.; Iqbal, J.; Mohsan, M. Screening for salt tolerance in maize (*Zea mays* L.) hybrids at an early seedling stage. *Pak. J. Bot.* **2010**, *42*, 141–154.
9. Liu, H.; Zhang, F.L.; Tian, H.J.; Hu, M.T.; Li, R.F.; Yang, X.D.; Zhang, D. Study on Salt Tolerance of Different Maize Varieties at Germination and Seedling Stages. *Seed* **2023**, *42*, 56–62+69.
10. Boote, K.J.; Kropff, M.J.; Bindraban, P.S. Physiology and modelling of traits in crop plants: Implications for genetic improvement. *Agric. Syst.* **2001**, *70*, 395–420. [CrossRef]
11. Asseng, S.; Ewert, F.; Martre, P.; Rötter, R.P.; Lobell, D.B.; Cammarano, D.; Kimball, B.A.; Ottman, M.J.; Wall, G.W.; White, J.W. Rising temperatures reduce global wheat production. *Nat. Clim. Change* **2015**, *5*, 143–147. [CrossRef]
12. Marcaida, I.M.; Li, T.; Angeles, O.; Evangelista, G.K.; Fontanilla, M.A.; Xu, J.; Gao, Y.; Li, Z.; Ali, J. Biomass accumulation and partitioning of newly developed Green Super Rice (GSR) cultivars under drought stress during the reproductive stage. *Field Crops Res.* **2014**, *162*, 30–38. [CrossRef]
13. Gouache, D.; Bogard, M.; Pegard, M.; Thepot, S.; Garcia, C.; Hourcade, D.; Paux, E.; Oury, F.; Rousset, M.; Deswarte, J. Bridging the gap between ideotype and genotype: Challenges and prospects for modelling as exemplified by the case of adapting wheat (*Triticum aestivum* L.) phenology to climate change in France. *Field Crops Res.* **2017**, *202*, 108–121. [CrossRef]
14. Semenov, M.A.; Stratonovitch, P. Designing high-yielding wheat ideotypes for a changing climate. *Food Energy Secur.* **2013**, *2*, 185–196. [CrossRef]

15. Martre, P.; He, J.; Le, G.J.; Semenov, M.A. In silico system analysis of physiological traits determining grain yield and protein concentration for wheat as influenced by climate and crop management. *J. Exp. Bot.* **2015**, *66*, 3581–3598. [CrossRef] [PubMed]
16. Rötter, R.P.; Tao, F.; Höhn, J.G.; Palosuo, T. Use of crop simulation modelling to aid ideotype design of future cereal cultivars. *J. Exp. Bot.* **2015**, *66*, 3463–3476. [CrossRef] [PubMed]
17. Tao, F.; Roetter, R.P.; Palosuo, T.; Diaz-Ambrona, C.G.H.; Minguez, M.I.; Semenov, M.A.; Kersebaum, K.C.; Nendel, C.; Cammarano, D.; Hoffmann, H.; et al. Designing future barley ideotypes using a crop model ensemble. *Eur. J. Agron.* **2017**, *82*, 144–162. [CrossRef]
18. Shahhosseini, M.; Hu, G.; Archontoulis, S.V. Forecasting corn yield with machine learning ensembles. *Front. Plant Sci.* **2020**, *11*, 1120. [CrossRef] [PubMed]
19. McNider, R.T.; Handyside, C.; Doty, K.; Ellenburg, W.L.; Cruise, J.F.; Christy, J.R.; Moss, D.; Sharda, V.; Hoogenboom, G.; Caldwell, P. An integrated crop and hydrologic modeling system to estimate hydrologic impacts of crop irrigation demands. *Environ. Model. Softw.* **2015**, *72*, 341–355. [CrossRef]
20. Xu, X.; Sun, C.; Neng, F.; Fu, J.; Huang, G. AHC: An integrated numerical model for simulating agroecosystem processes—Model description and application. *Ecol. Model.* **2018**, *390*, 23–39. [CrossRef]
21. Wang, W.; Huo, Z.; Rong, Y.; Wang, C.Z.; Zhang, C.L.; Wang, X.W. A novel water use efficiency model based on stomata coupling crop growth and farmland water cycle processes in arid areas. *J. Hydrol.* **2023**, *617*, 128974. [CrossRef]
22. Gao, Y.; Zhang, H.; Xue, Y.; Kuang, P.; Qian, X.; Dai, H.; Li, Y.; Wang, Z.; Han, X.; Li, Z. Comprehensive evaluation of salt tolerance and screening for salt tolerance accessions of different summer maize varieties. *J. Maize Sci.* **2020**, *28*, 33–40.
23. Wang, X.; Zhang, H.; Pan, X.; Liu, G.; Zhao, Y. Evaluation of salt tolerance and selection of salt tolerant germplasm in maize at adult stage. *Mol. Plant Breed.* **2020**, *18*, 685–692.
24. Ma, Z.; Liu, J.; Wu, N.; Yang, Y.; Hu, Y.; Zhe, Y. Effects of Deep Rotary Tillage Combined with Organic Fertilizer on Bacterial Community Structure and Function of Maize Rhizosphere Soil in Saline Alkali Land. *Chin. J. Agrometeorol.* **2023**, *44*, 479–491.
25. Balboa, G.R.; Archontoulis, S.V.; Salvagiotti, F.; Garcia, F.O.; Stewart, W.M.; Francisco, E.; Prasad, P.V.; Ciampitti, I.A. A systems-level yield gap assessment of maize-soybean rotation under high-and low-management inputs in the Western US Corn Belt using APSIM. *Agric. Syst.* **2019**, *174*, 145–154. [CrossRef]
26. Corbeels, M.; Chirat, G.; Messad, S.; Thierfelder, C. Performance and sensitivity of the DSSAT crop growth model in simulating maize yield under conservation agriculture. *Eur. J. Agron.* **2016**, *76*, 41–53. [CrossRef]
27. Jones, J.W.; Hoogenboom, G.; Porter, C.H.; Boote, K.J.; Batchelor, W.D.; Hunt, L.A.; Wilkens, P.W.; Singh, U.; Gijsman, A.J.; Ritchie, J.T. The DSSAT cropping system model. *Eur. J. Agron.* **2003**, *18*, 235–265. [CrossRef]
28. Jones, J.W.; He, J.; Boote, K.J.; Wilkens, P.; Porter, C.H.; Hu, Z. Estimating DSSAT cropping system cultivar-specific parameters using Bayesian techniques. *Methods Introd. Syst. Models Into Agric. Res.* **2011**, *2*, 365–393.
29. Keating, B.A.; Carberry, P.S.; Hammer, G.L.; Probert, M.E.; Robertson, M.J.; Holzworth, D.; Huth, N.I.; Hargreaves, J.N.; Meinke, H.; Hochman, Z. An overview of APSIM, a model designed for farming systems simulation. *Eur. J. Agron.* **2003**, *18*, 267–288. [CrossRef]
30. Malone, R.W.; Huth, N.; Carberry, P.S.; Ma, L.; Kaspar, T.C.; Karlen, D.L.; Meade, T.; Kanwar, R.S.; Heilman, P. Evaluating and predicting agricultural management effects under tile drainage using modified APSIM. *Geoderma* **2007**, *140*, 310–322. [CrossRef]

Disclaimer/Publisher's Note: The statements, opinions and data contained in all publications are solely those of the individual author(s) and contributor(s) and not of MDPI and/or the editor(s). MDPI and/or the editor(s) disclaim responsibility for any injury to people or property resulting from any ideas, methods, instructions or products referred to in the content.